Unsteady free convection flow of water-based carbon nanotubes due to non-coaxial rotations of moving disk

Wan Nura'in Nabilah Noranuar[1], Ahmad Qushairi Mohamad[1*], Sharidan Shafie[1], and Ilas Khan[2]

[1] *Department of Mathematical Sciences, Faculty of Science, Universiti Teknologi Malaysia, 81310 Johor Bahru, Johor, Malaysia*
[2] *Basic Engineering Sciences Department, College of Engineering Majmaah University, Majmaah 11952, Saudi Arabia*
[*] *Corresponding author. E-mail: ahmadqushairi@utm.my*

Received: Dec. 06, 2020; Accepted: Feb. 19, 2021

Nanofluid is one of the significant developments for having an efficient heat transport process. Its implementation in a non-coaxial rotating system has benefited from designing a mixer machine with two stirrer blades, cooling fan, and jet engines. This study analytically investigates the free convection of unsteady non-coaxial rotating nanofluid flow through a moving disk. The suspension of single-wall or multi-wall carbon nanotubes in water is known as the nanofluid in this study. The fluid motion is affected by the effects of rotation and buoyancy forces. Using suitable dimensionless variables, the dimensional coupled partial differential of momentum and energy equations along with their initial and moving boundary conditions are converted into the dimensionless form. The expressions for temperature and velocity profiles are obtained by solving governing equations using Laplace transform method. The validity of obtained solution is confirmed by having a good agreement when comparing present results with the published result. The results show that the insertion of CNTs particles into the rotating water causes the temperature and velocity profiles to increase. The amount of heat transferred by SWCNTs is greater than MWCNTs. Increasing CNTs particles has descended both primary and secondary skin friction but increase Nusselt number. Further analysis with the help of pictorial discussion for the fluid flows and heat transfer under the influences of nanoparticle volume fraction, Grashof number, the amplitude of disk, and time is carried out.

Keywords: Non-coaxial rotation, Nanofluid, Carbon nanotubes, Laplace transform method, Moving disk

http://dx.doi.org/10.6180/jase.202206_25(3).0005

1. Introduction

Recently, the advancement of heat transfer systems among emergence industries has created a significant demand for a new technology to improve their heat transfer process. The implementation of nanofluid is an alternative for industries to have an efficient heat transfer system. The development of nanofluid as a smart heat transfer fluid by dispersing nanoparticles in the conventional base fluid was initiated by Choi and Eastman [1]. The conventional base fluid is reported to have limited capabilities in heat transfer. Generally, nanoparticles, a nano-sized material with unique chemical and physical properties such as metals, metal oxides, or carbon, are immersed in this fluid to enhance the nanofluid thermal conductivity. Hence, the process of conduction and convection be more effective in transferring heat [2]. The great potential of nanofluid in the promising enhancement of heat transfer has encouraged many researchers into this interest. The study of nanofluid flow features using ordinary nanoparticles like Cu, Ag, CuO, Al_2O_3 and TiO_2, over a moving plate with various effects were available in [3–5]. One of the developments in nanofluid is carbon nanotubes (CNTs), and it is mainly found in two

types, which are single-wall carbon nanotubes (SWCNTs) and multi-wall carbon nanotubes (MWCNTs). Specifically, SWCNTs are known as the cylindrical tubes made up of a single layer of 0.4-3nm diameter of graphene sheet, while MWCNTs are structured by a group of nested tubes multi-layer of a graphene sheet and have a diameter in the range of 0.4 to 30nm [6]. Due to their outstanding properties, CNTs have gained tremendous attention from scientists and engineers. They are widely found in various applications such as designing electronic devices, sensors and transistors, and in the medical field, drug delivery transport, tissue engineering, and biomedical imaging. Khalid et al. [7] performed the study on oscillating nanofluid with CNTs flow, and the problem is solved by applying Laplace transform method. The previous study [7] was extended by Khalid et al. [8], considering the mixture of human blood and CNTs as the nanofluid. The thermal field and flow features across coiled stretching sheet affected by CNTs was unfolded by Acharya et al. [9]. Mahanthesh et al. [10] discussed the impacts of CNTs nanofluid on MHD radiative Marangoni convection and found that the heat transfer is enhanced with CNTs. A numerical analysis on Brinkman-Forchheimer flow with CNTs suspension over a microchannel was conducted by Shashikumar et al. [11]. Shehzad et al. [12] improved the previous study [11] by including thermal and exponential space-dependent heat sources. More related studies of flow characteristics on CNTs nanofluid with various geometries were presented by [13–16].

The fluid dynamic and heat transport subjected to a rotating system had recently fascinated significant attention from numerous investigators. Its modeling and rheology can be implemented in engineering processes, especially designing the rotating machinery component such as vacuum cleaners, pumps, jet engines, and cooling turbine blades. Acharya [17] investigated the steady-state of MHD CNTs nanofluid flow over a rotating disk. A similar study as in [17] was conducted by Acharya [18], which considering the flow is unsteady and is imposed with a highly oscillating magnetic field. Both studies [17, 18] reported that MWCNTs have a prominent effect on velocity compared to SWCNTs. The features of hybrid nanofluid flow induced by rotating disk were analyzed by Gowda et al. [19] and Jayadevamurthy et al. [20], where the upward and downward motion of the disk were imposed. Acharya et al. [21] also conducted a similar analysis as in [20] on MHD flow and radiative spinning disk. The impact of immersing CNTs in water-based fluid on a rotating system flow was discovered by Acharya et al. [22], considering the stretching sheet problem, while Rehman et al. [23] considering the problem of two parallel plates. Mahanthesh et al. [24] determined the flow of CNTs suspension using a stretchable type of rotating disk. Kotresh et al. [25] also adopted the stretchable rotating disk to investigate the heat propagation and fluid flow in the presence of magnetic field, chemical response and activation energy.

The above review on rotating flow has indicated that the idea of non-coaxial rotation type has not been emphasized. However, a similar study related to this type of rotation was conducted by Mahanthesh et al. [24] to determine the non-linear density fluctuation of Casson fluid with heat and mass transfer effects. Mohamad et al. [26] discussed the non-coaxial rotation of Newtonian fluid flow executed by oscillating disk. Ersoy [27] improved the previous study by considering the MHD effect on periodic flow, and the disk oscillates non-torsionally. The study of non-coaxial rotation with an accelerated disk of viscous fluid together with MHD and porosity effects is discussed by Mohamad et al. [26] and Laplace transform method was utilized to get the exact solutions. The implementation of non-coaxial rotating flow in nanofluid in the presence of MHD, porosity, and suction was conducted by Das et al. [28]. Most recently, Ashlin and Mahanthesh [29] discovered the features of non-coaxial rotation flow with the aid of hybrid nanofluid suspension.

Based on the above literature, it is found that the impact of CNTs suspension on non-coaxial rotating flow is not yet explored by any researchers. Therefore, it is undeniable that the investigation of the unsteady flow of CNTs nanofluid affected by non-coaxial rotation will be a new contribution in the light of overcoming the limited access to this field. In other words, the current investigation is motivated by the previous work to analyze the free convection flow of water-based CNTs with non-coaxial rotation induced by a moving vertical disk. By using the method of Laplace transform, the exact solutions for the problem are analytically solved. The results for the temperature and velocity are plotted and analyzed for pertinent embedded parameters.

2. Description of problem formulation

Consider the non-coaxial rotation of an incompressible Newtonian nanofluid is unsteadily flow by free convection with a moving vertical disk. The upward direction is referred to the x-axis of the disk, while normal to the plane of disk is referred to the z-axis. The medium of embedded disk is filled with a mixture of water and SWCNTs or a mixture of water and MWCNTs. Both disk and nanofluid have rotate, and their axes are considered to be in plane $x = 0$. When $t = 0$, both nanofluid and disk initially rotate on

z′-axis with a similar angular velocity Ω and temperature T_∞. Later, when t >0, the disk starts to move and rotate on z-axis, while the nanofluid at infinity remains to rotate on z′-axis. Both rotations have a similar angular velocity Ω with the temperature of the disk raises to T_w. The two axes of rotation are separated by a distance, known as l. The schematic diagram explaining to the problem is shown in Fig. 1. The governing equations on non-coaxial rotation of Newtonian nanofluid flow is given as [26].

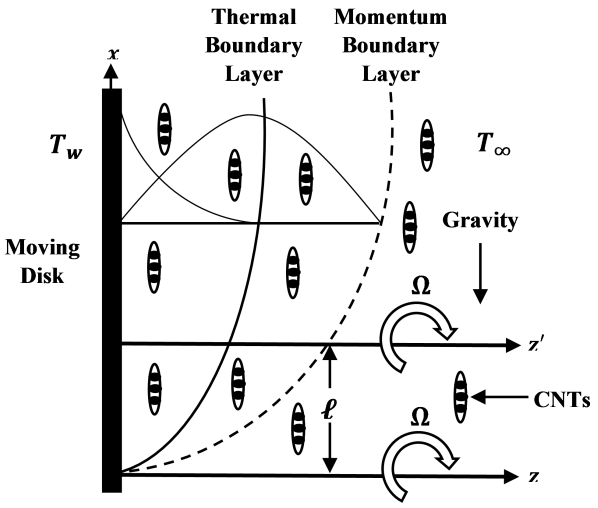

Fig. 1. Schematic diagram of the problem.

$$\rho_{nf}\frac{\partial F}{\partial t}+\rho_{nf}\Omega iF=\mu_{nf}\frac{\partial^2 F}{\partial z^2}+\rho_{nf}\Omega^2 il+(\rho\beta_T)_{nf}g_x(T-T_\infty) \tag{1}$$

$$(\rho C_p)_{nf}\frac{\partial T}{\partial t}=k_{nf}\frac{\partial^2 T}{\partial z^2} \tag{2}$$

together with initial and boundary conditions

$$\begin{array}{lll} F(z,0)=\Omega l, & T(z,0)=T_\infty & \forall z>0 \\ F(0,t)=U_0 & T(0,t)=T_w & \forall t>0 \\ F(\infty,t)=\Omega l & T(\infty,t)=T_\infty & \forall t>0 \end{array} \tag{3}$$

where $F=f+g$ is the nanofluid velocity in complex form, which f is the primary velocity (real part) and g is the secondary velocity (imaginary part), respectively, and T is the nanofluid temperature. Meanwhile, k_{nf}, μ_{nf}, ρ_{nf}, $(\rho C_p)_{nf}$, $(\beta_T)_{nf}$ are thermal conductivity, dynamic viscosity, density, heat capacitance, thermal expansion coefficient for temperature, which specifically for nanofluid and U_0 is the characteristic velocity.

The nanofluid thermal conductivity and rate of dimensionless heat transfer in this study are analyzed by applying the theoretical model introduced by Xue [30]. This model is established based on Maxwell theory by taking into account the rotating elliptical nanotubes with a substantial axial ratio and offsetting the space distribution impacts on CNTs. The thermal conductivity of CNTs nanofluid is greatly affected by this model because its small amount of CNTs dispersion can result a significant enhancement in the thermal conductivity of CNTs rotating nanofluid. Thus, the model is given as [7–9, 12, 22].

$$\begin{aligned} &\mu_{nf}=\frac{\mu_f}{(1-\phi)^{2.5}},\ \beta_{nf}=\frac{(1-\phi)(\rho\beta)_f+\phi(\rho\beta)_{CNTs}}{\rho_{nf}}, \\ &\rho_{nf}=(1-\phi)\rho_f+\phi\rho_{CNTs}, \\ &(\rho C_p)_{nf}=(1-\phi)(\rho C_p)_f+\phi(\rho C_p)_{CNTs}, \\ &\frac{\sigma_{nf}}{\sigma_f}=\left\{1+\frac{3(\frac{\sigma_{CNTs}}{\sigma_f}-1)\phi}{(\frac{\sigma_{CNTs}}{\sigma_f}+2)-\phi(\frac{\sigma_{CNTs}}{\sigma_f}-1)}\right\}, \\ &\lambda=\frac{k_{nf}}{k_f}=\frac{1-\phi+2\phi\frac{k_{CNTs}}{k_{CNTs}-k_f}ln\frac{k_{CNTs}+k_f}{2k_f}}{1-\phi+2\phi\frac{k_f}{k_{CNTs}-k_f}ln\frac{k_{CNTs}+k_f}{2k_f}} \end{aligned} \tag{4}$$

where the subscripts $CNTs$ and f indicate to carbon nanotubes and fluid, and ϕ is the nanofluid solid volume fraction, which afterwards are used based on their particular thermophysical properties as tabulated in Table 1.

The following dimensionless variables are introduced [26]:

$$F^*=\frac{F}{\Omega l}-1,\ z^*=\sqrt{\frac{\Omega}{v}}z,\ t^*=\Omega t,\ T^*=\frac{T-T_\infty}{T_w-T_\infty} \tag{5}$$

After substituting variables in Eq. 5 and employing nanofluid model in Eq. 4, the system of Eqs. 1 – 3 reduces to

$$\frac{\partial F}{\partial t}+iF=\frac{1}{\phi_1}\frac{\partial^2 F}{\partial z^2}+\phi_2 GrT \tag{6}$$

$$\frac{\partial T}{\partial t}=\frac{1}{a_0}\frac{\partial^2 T}{\partial z^2} \tag{7}$$

subjected to the dimensionless conditions

$$\begin{array}{lll} F(z,0)=0, & T(z,0)=0 & \forall z>0 \\ F(0,t)=U-1 & T(0,t)=1 & \forall t>0 \\ F(\infty,t)=0 & T(\infty,t)=0 & \forall t>0 \end{array} \tag{8}$$

where $Pr=\frac{v_f(\rho C_p)_f}{k_f}$, $Gr=\frac{g_x\beta_{T_f}(T_w-T_\infty)}{\Omega^2 l}$, $U=\frac{U_0}{\Omega l}$ are Prandtl number, Grashof number and amplitude of disk. For other constant parameters are defined as:

$$\begin{aligned} &a_0=\frac{Pr\phi_3}{\lambda},\ \phi_1=(1-\phi)^{2.5}((1-\phi)+\frac{\phi\rho_{CNTs}}{\rho_f}, \\ &\phi_2=\frac{(1-\phi)+\frac{\phi(\rho\beta)_{CNTs}}{(\rho\beta)_f}}{(1-\phi)+\frac{\phi\rho_{CNTs}}{\rho_f}},\ \phi_3=(1-\phi)+\frac{\phi(\rho C_p)_{CNTs}}{(\rho C_p)_f} \end{aligned}$$

Table 1. Thermophysical properties of water, SWCNTs, and MWCNTs.

MaterialsProperties	$\rho(Kgm^{-3})$	$C_p(JKg^{-1}K^{-1})$	$k(Wm^{-1}K^{-1})$	$\sigma(Sm^{-1})$	$\beta \times 10^{-5}(K^{-1})$
Water	997.1	4179	0.613	21x10^{-5}	0.05
SWCNTs	2600	425	6600	27x10^{-5}	10^{6}-10^{7}
MWCNTs	1600	796	3000	44x10^{-5}	1.9x10^{-4}

3. Analytical solution of the problem

Making use of Laplace transform method, Eqs. 6 and 7 together with the conditions 8 transforms to

$$\frac{\mathrm{d}^2}{\mathrm{d}z^2}\bar{F}(z,q) - (\phi_1 q + \phi_1 i)\bar{F}(z,q) = -m_1 Gr \frac{1}{q} exp(-z\sqrt{a_0 q}) \tag{9}$$

$$\bar{F}(0,q) = (U-1)\frac{1}{q},\ \bar{F}(\infty,q) = 0 \tag{10}$$

$$\frac{\mathrm{d}^2}{\mathrm{d}z^2}\bar{T}(z,q) - (a_0 q)\bar{T}(z,q) = 0 \tag{11}$$

$$\bar{T}(0,q) = \frac{1}{q},\ \bar{T}(\infty,q) = 0 \tag{12}$$

Then, the conditions 10 and 12 are used to solve Eqs. 9 and 11. After that, by applying inverse Laplace transform, the resulting velocity and temperature solutions lead to

$$F(z,t) = F_1(z,t) - F_2(z,t) - F_3(z,t) + F_4(z,t) + F_5(z,t) - F_6(z,t) \tag{13}$$

$$T(z,t) = erfc\left(\frac{z}{2}\sqrt{\frac{a_0}{t}}\right) \tag{14}$$

with

$$F_1(z,t) = \frac{1}{2}U\left[exp(z\sqrt{d_2 i})erfc\left(\frac{z}{2}\sqrt{\frac{\phi_1}{y}} + \sqrt{\phi_1 it}\right) + exp(-z\sqrt{d_2 i})erfc\left(\frac{z}{2}\sqrt{\frac{\phi_1}{t}} - \sqrt{\phi_1 it}\right)\right],$$

$$F_2(z,t) = \frac{1}{2}\left[exp(z\sqrt{d_2 i})erfc\left(\frac{z}{2}\sqrt{\frac{\phi_1}{y}} + \sqrt{\phi_1 it}\right) + exp(-z\sqrt{d_2 i})erfc\left(\frac{z}{2}\sqrt{\frac{\phi_1}{t}} - \sqrt{\phi_1 it}\right)\right]$$

$$F_3(z,t) = \frac{1}{2}a_4[exp(z\sqrt{d_2 i})erfc(\frac{z}{2}\sqrt{\frac{\phi_1}{y}} + \sqrt{\phi_1 it}) + exp(-z\sqrt{d_2 i})erfc(\frac{z}{2}\sqrt{\frac{\phi_1}{t}} - \sqrt{\phi_1 it})]$$

$$F_4(z,t) = \frac{1}{2}a_4\begin{bmatrix} exp(a_3 t + z\sqrt{d_2 i})erfc(\frac{z}{2}\sqrt{\frac{\phi_1}{t}} + \sqrt{(a_3+\phi_1 i)t})) + \\ exp(a_3 t + z\sqrt{d_2 i})erfc(\frac{z}{2}\sqrt{\frac{\phi_1}{t}} + \sqrt{(a_3+\phi_1 i)t})) + \end{bmatrix}$$

$$F_5(z,t) = a_4 erfc(\frac{z}{2}\sqrt{\frac{a_0}{t}}$$

$$F_6(z,t) = \frac{1}{2}a_4[exp(a_3 t + z\sqrt{a_0 a_3})erfc(\frac{z}{2}\sqrt{\frac{a_0}{t}} + \sqrt{a_3 t}) + exp(a_3 t - z\sqrt{a_0 a_3})erfc(\frac{z}{2}\sqrt{\frac{a_0}{t}} - \sqrt{a_3 t})]$$

where $a_1 = \phi_1\phi_2$, $a_2 = a_0 - \phi_1$, $a_3 = \frac{\phi_1 i}{a_2}$, $a_4 = \frac{a_1 Gr}{a_2 a_3}$, and $d_2 = \phi_1\phi_1$

4. Skin friction and Nusselt number

The skin friction and rate of heat transfer by Nusselt number τ are the significant physical quantities in engineering and industry field. It is expressed as [24]:

$$\tau = \frac{1}{(1-\phi)^{2.5}}\left[\frac{\partial F}{\partial z}\right]_{z=0} \tag{15}$$

and

$$\tau = \frac{k_{nf}}{k_f}\left[\frac{\partial T}{\partial z}\right]_{z=0} \tag{16}$$

5. Results and discussion

At this part, the heat transfer and non-coaxial rotating nanofluid flow regimes are further analyzed by graphically plotting the solutions 13 – 14, as presented in Fig. 2 to 8 based on the thermophysical properties in Table 1. The nanoparticle volume fraction ϕ, Grashof number Gr, amplitude of disk U, and time t effects are investigated for different numerical values with the value for physical parameters are set to Pr=6.2, Gr=0.5, ϕ=0.02, t=0.2, and U =2 [4, 7, 8, 16, 26]. For a rotating fluid, the velocity profile is presented in a complex form where the real and imaginary parts respectively indicate the primary f and secondary g velocities. The results for primary τ_p and secondary skin friction τ_s and Nusselt number Nu with various parameters are tabulated in Tables 2 and 3.

Based on Fig. 2, the impact of ϕ on primary and secondary velocities for SWCNTs and MWCNTs are presented,

Table 2. Variant of skin friction for embedded parameters at Pr=6.2.

ϕ	Gr	t	U	SWCNTs		MWCNTs	
				τ_p	τ_s	τ_p	τ_s
0.02	0.5	0.2	2	-1.239	-0.264	-1.226	-0.262
0.12	0.5	0.2	2	-1.483	-0.327	-1.398	-0.310
0.22	0.5	0.2	2	-1.803	-0.407	-1.627	-0.372
0.02	5	0.2	2	-0.476	-0.280	-0.468	-0.278
0.02	10	0.2	2	0.371	-0.298	0.375	-0.295
0.02	0.5	0.4	2	-0.835	-0.375	-0.826	-0.371
0.02	0.5	0.6	2	-0.658	-0.459	-0.651	-0.455
0.5	0.02	0.2	3	-2.562	-0.527	-2.536	-0.522
0.5	0.02	0.2	4	-3.885	-0.789	-3.847	-0.782

Table 3. Variant of skin friction for embedded parameters at Pr=6.2.

ϕ	t	Nu	
		SWCNTs)	MWCNTs)
0.02	0.2	3.624	3.582
0.12	0.2	5.484	5.318
0.22	0.2	6.953	6.718
0.02	0.4	2.562	2.533
0.02	0.6	2.092	2.068

where an increment of ϕ reports an increase in f profile (SWCNTs and MWCNTs). For g profiles (SWCNTs and MWCNTs), the fluctuating trend is noticed. Its enhancement for increasing ϕ is exhibited when 0.5, and the maximum secondary velocity is reported when z=0.5. The velocity escalation is noticed much higher in the case of MWCNTs than SWCNTs. Skin friction (τ_p and τ_s) for both SWCNTs and MWCNTs in Table 2 decreases as ϕ is enriched. The temperature profile under the impact of ϕ is depicted in Fig. 3. It shows that the temperature of nanofluid raises with the insertion of more CNTs. This is because the implementation of CNTs amplifies the nanofluid thermal conductivity, which then improves nanofluid's ability to conduct heat. Such behavior proves that the fluid containing a high volume of CNTs can conduct more heat, resulting in an increased temperature profile and thickening of the thermal boundary layer. This particular behavior under the impact of CNTs is also discussed by Ebaid and Al-Sharif [15] and Acharya et al. [22]. The maximum temperature of nanofluid is found when the fluid is near the surface due to the imposed wall temperature, and it subsequently drops when the fluid moves far away from the surface. In addition to the impact of ϕ, Table 3 shows that ascending ϕ increases the rate of heat transfer for both SWCNTs and MWCNTs suspension. This effect is possible because increasing ϕ reduces the nanofluid's heat capacity and hence, the thermal energy transfer will take at a high rate. SWCNTs also record a higher enhancement rate compared to MWCNTs. Thus, SWCNTs can be the ideal candidates for having an effective thermal energy transmission system.

Furthermore, the influence of Gr on f and g profiles (SWCNTs and MWCNTs) is shown in Fig. 5. It reveals that both f and g profiles (SWCNTs and MWCNTs) elevate with ascending values of Gr, which it has also been discovered by Saqib et al. [16]. When Gr ascends, it implies to the temperature growth and causes the buoyancy force to dominate the flow. As a result, the fluid becomes less viscous, and both f and g profiles elevate, which can be clearly observed within the interval $0 \leq z \leq 1$. A clear pictorial view of SWCNTs and MWCNTs effects is presented at the zooming box. The magnitude of velocity for SWCNTs is slower than MWCNTs, which is greatly influenced by a high density of SWCNTs. Table 2 shows another impact of rising Gr values, which also causes τ_p to increase and τ_s to decrease.

Next, an identical behavior of f and g profiles (SWCNTs and MWCNTs) is depicted under the influence of t as in Fig. 6, whereby an increase in t escalates both f and g profiles (SWCNTs and MWCNTs). It is useful to note that when a longer time, the external source, which is created by the moving disk, continuously supplies the energy to the flow, and consequently, causes velocity and temperature (SWCNTs and MWCNTs) to increase, as shown in Fig. 4. This effect is followed by an increase of the thermal boundary layer and the reduction of heat transfer rate, as clearly presented in Table 3. Meanwhile, Table 2 observes that as t increases, the enhancement of τ_p and the declination of τ_s have occurred. This impact causes large drag effect at the surface is experienced by primary profile compared to secondary profile. Fig. 7 proves that the amplification in U also contributes in the increase of and profiles (SWCNTs and MWCNTs), and diminishes both τ_p and τ_s (SWCNTs and MWCNTs). This is because the moving disk is the external forces that apply force to rotate the fluid and increase the friction between fluid and disk. Besides, this force helps CNTs to provide fully reaction at all regions of rotating fluid. This trend of velocity profiles affected by the increase of t and U is also reported by Anwar et al. [4], Mahanthesh et al. [24] and Mohamad et al. [26]. For both t and U influences, the effect between SWCNTs and MWCNTs is insignificantly seen. However, its difference can be discovered inside the zooming box. It shows that SWCNTs exhibits a lower velocity profile and higher temperature profile compared to MWCNTs.

Overall, from Fig. 2 to 7, it can be concluded that f and g profiles for MWCNTs are higher than SWCNTs due to the

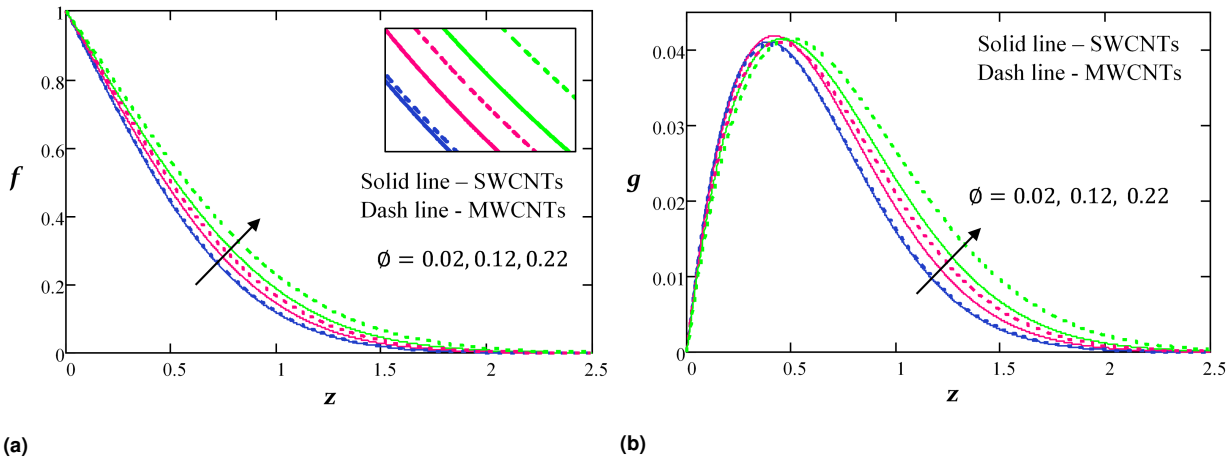

Fig. 2. f and g profiles under the impact of different ϕ values.

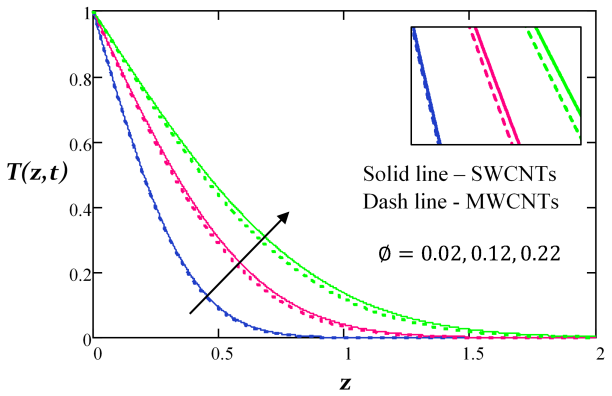

Fig. 3. Temperature profile under the impact of different ϕ values.

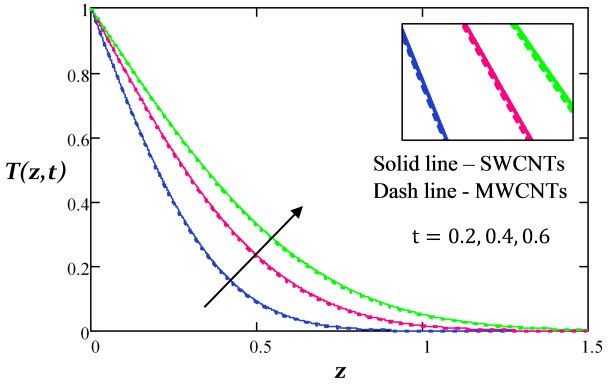

Fig. 4. Temperature profile under the impact of different t values.

low density of MWCNTs while the temperature for SWCNTs is higher than MWCNTs because SWCNTs has a high thermal conductivity. The similar effects of SWCNTs and MWCNTs on velocity and temperature were also found in Ebaid and Al Sharif [15], Acharya et al. [22], and Mahanthesh et al. [24]. Lastly, the published work by Mohamad et al. [26] is used to verify the obtained solutions, and its comparison for primary and secondary velocities is carried out as depicted in Fig. 8. While, Tables 5 and 5 show the comparison for skin friction and Nusselt number, respectively. Another comparison of exact solutions 13 with Mohamad et al. [26] and numerical results by Gaver–Stehfest algorithm [31, 32] is also conducted and tabulated in Table 6. This algorithm provides a numerical inversion of Laplace transform and its numerical values is used to compare with the exact solutions. The validity is confirmed when the identical result is achieved for all comparisons between the present results and Mohamad et al. [26] as well as with Gaver–Stehfest Algorithm, by allowing ω=0 in Mohamad et al. [26] and ϕ=0 in present results.

6. Conclusions

The exact solutions for the unsteady free convection of Newtonian nanofluid flow with carbon nanotubes over a moving disk are accomplished by applying Laplace transform method. The influence of embedded parameters with different numerical values on both temperature and velocity profiles are illustrated graphically, and the significant points observed in this study are

- An increase value of nanoparticle volume fraction, Grashof number, time, and disk amplitude causes both primary and secondary velocity profiles to increase.
- An increase value of nanoparticle volume fraction and time increases the nanofluid temperature profile.
- For both primary and secondary velocity profiles,

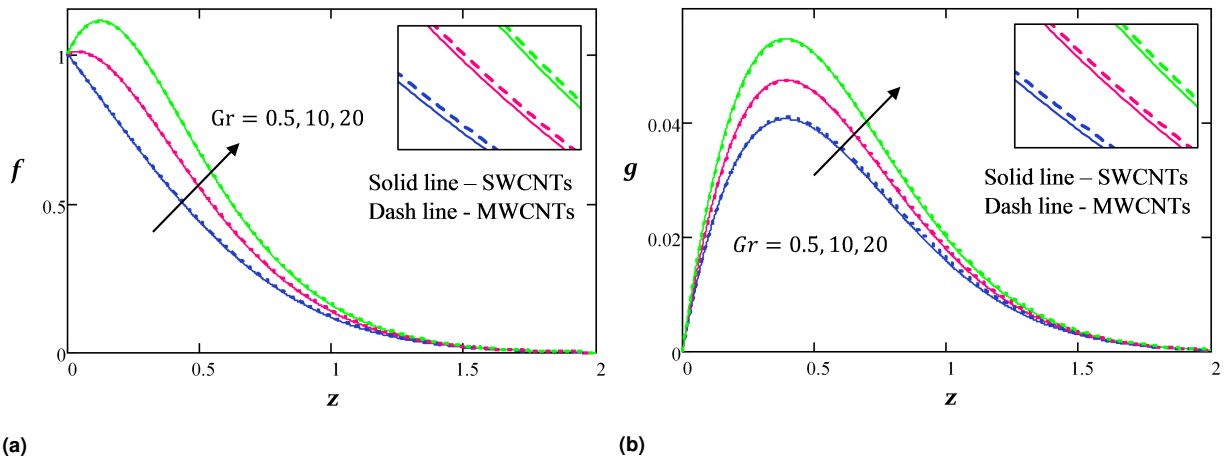

(a) (b)

Fig. 5. f and g profiles under the impact of different Gr values.

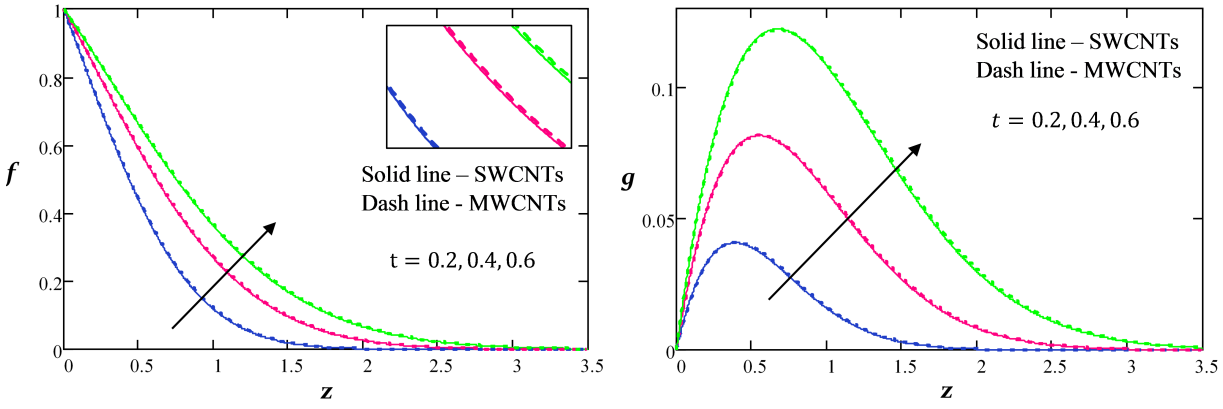

(a) (b)

Fig. 6. f and g profiles under the impact of different t values.

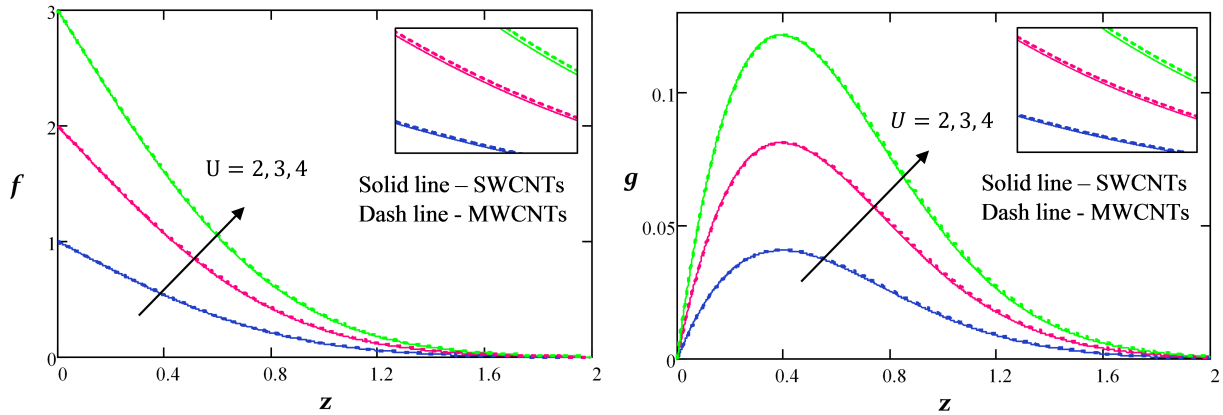

(a) (b)

Fig. 7. f and g profiles under the impact of different U values.

nanofluid with MWCNTs is prominent compared to SWCNTs due to their low density.

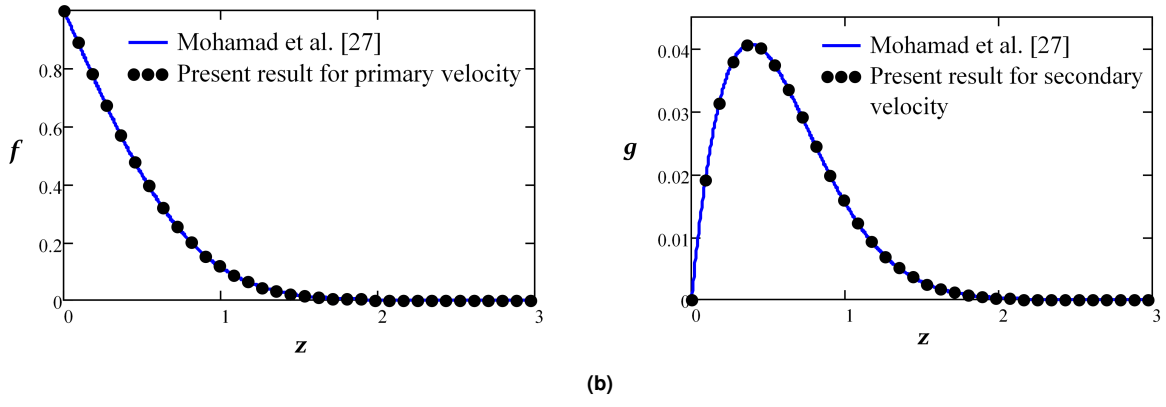

Fig. 8. Verification of present results with published results from Mohamad et al. [26].

Table 4. Comparison of skin friction values at Pr=6.2.

Gr	U	t	Present results $\phi = 0$		Mohamad et al. [26] $\omega = 0$	
			τ_p	τ_s	τ_p	τ_s
0.5	2	0.2	-1.197712	-0.253357	-1.197712	-0.253357
5	2	0.2	-0.547434	-0.265774	-0.547434	-0.265774
10	2	0.2	0.175097	-0.279570	0.175097	-0.279570
0.5	3	0.2	-2.467676	-0.505334	-2.467676	-0.505334
0.5	4	0.2	-3.737641	-0.757311	-3.737641	-0.757311
0.5	2	0.4	-0.813717	-0.358821	-0.813717	-0.358821
0.5	2	0.6	-0.646961	-0.438940	-0.646961	-0.438940

Table 5. Comparison of Nusselt number values at Pr=6.2.

t	Nu	
	Present results $\phi = 0$	Mohamad et al [26] $\omega = 0$
0.2	3.141275	3.141275
0.4	2.221217	2.221217
0.6	1.813616	1.813616

- For temperature profile, nanofluid with SWCNTs is prominent compared to MWCNTs due to its high thermal conductivity.
- As nanoparticle volume fraction ascends, Nusselt number for both SWCNTs and MWCNTs increase due to nanofluid heat capacity diminution. While, as time ascends, Nusselt number for both SWCNTs and MWCNTs decreases.
- Both primary and secondary skin friction decline when the values of nanoparticle volume fraction and disk amplitude increase. While, increasing Grashof number and time cause an enhancement in primary skin friction and a reduction in secondary skin friction.
- An excellent agreement is obtained between the present results and Mohamad et al. [26] as well as with Gaver–Stehfest algorithm. Hence, the validity of obtained solution is verified.

7. Acknowledgements

The authors would like to acknowledge Ministry of Education (MOE) and Research Management Centre-UTM, Universiti Teknologi Malaysia (UTM) for the financial support through vote numbers 17J98, 5F004, 5F278, 07G70, 07G72, 07G76, 07G77, 08G33 and 4B583 for this research.

8. Nomenclature

β: Thermal expansion coefficient (K^{-1})
β_T: Thermal expansion coefficient for temperature (K^{-1})
C_p: Specific heat (J kg^{-1} K^{-1})
g_x: Acceleration due to gravity (m s^{-2})
F: Complex velocity of nanofluid (m s^{-1})
f: Primary velocity of nanofluid (m s^{-1})
g: Secondary velocity of nanofluid (m s^{-1})
k: Thermal conductivity (W m^{-1} K^{-1})
T_w: Wall temperature (K)
T_∞: Free stream temperature (K)
T: Temperature of nanofluid (K)
U_0: Characteristic of velocity (m s^{-1})
U: Amplitude of disk (m s^{-1})
t: Time (s)
i: Imaginary unit
Pr: Prandtl number
Nu: Nusselt number
Gr: Grashof number
μ: Dynamic viscosity (kg m s^{-1})
ρ: Density (kg m^{-3})
ϕ: Nanofluid solid volume fraction
τ: Skin friction
σ: Electrical conductivity (S m^{-1})
Ω: Angular velocity (rad s^{-1})

Table 6. Comparison of velocity solutions 13 (ϕ=0) with Mohamad et al. [26] (ω=0) and Gaver–Stehfest algorithm.

z	Gr	t	U	Primary velocity			Secondary velocity		
				Present results 13	Mohamad et al. [27]	Gaver-Stehfest	Present results 13	Mohamad et al. [26]	Gaver-Stehfest
0	0.5	0.2	2	1.0000	1.0000	1.0000	0.0000	0.0000	0.0000
0.5	0.5	0.2	2	0.4312	0.4312	0.4312	0.0388	0.0388	0.0388
1.0	0.5	0.2	2	0.1134	0.1134	0.1134	0.0154	0.0154	0.0154
1.5	0.5	0.2	2	0.0176	0.0176	0.0176	0.0028	0.0028	0.0028
2.0	0.5	0.2	2	0.0015	0.0015	0.0015	0.0003	0.0003	0.0003

CNTs: Carbon nanotubes
nf: Nanofluid
f: Fluid

References

[1] S. U. Choi. "Enhancing thermal conductivity of fluids with nanoparticles". In: *American Society of Mechanical Engineers, Fluids Engineering Division (Publication) FED*. ***231***. 1995, 99–105.

[2] P. Sivashanmugam. "Application of Nanofluids in Heat Transfer". In: *An Overview of Heat Transfer Phenomena*. 2012. DOI: 10.5772/52496.

[3] , (2019) *"Free convection flow of nanofluid over infinite vertical plate with damped thermal flux"* **Chinese Journal of Physics *59***: 175–188. DOI: 10.1016/j.cjph.2019.02.029.

[4] T. Anwar, P. Kumam, Z. Shah, W. Watthayu, and P. Thounthong, (2020) *"Unsteady radiative natural convective MHD nanofluid flow past a porous moving vertical plate with heat source/sink"* **Molecules *25***(4): DOI: 10.3390/molecules25040854.

[5] W. A. Azhar, D. Vieru, and C. Fetecau, (2017) *"Free convection flow of some fractional nanofluids over a moving vertical plate with uniform heat flux and heat source"* **Physics of Fluids *29***(8): DOI: 10.1063/1.4996034.

[6] S. Nasir, Z. Shah, S. Islam, W. Khan, and S. N. Khan, (2019) *"Radiative flow of magneto hydrodynamics single-walled carbon nanotube over a convectively heated stretchable rotating disk with velocity slip effect"* **Advances in Mechanical Engineering *11***(3): DOI: 10.1177/1687814019827713.

[7] A. Khalid, L. Y. Jiann, I. Khan, and S. Shafie. "Exact solutions for unsteady free convection flow of carbon nanotubes over an oscillating vertical plate". In: *AIP Conference Proceedings*. ***1830***. 2017. DOI: 10.1063/1.4980917.

[8] A. Khalid, I. Khan, A. Khan, S. Shafie, and I. Tlili, (2018) *"Case study of MHD blood flow in a porous medium with CNTS and thermal analysis"* **Case Studies in Thermal Engineering *12***: 374–380. DOI: 10.1016/j.csite.2018.04.004.

[9] N. Acharya, R. Bag, and P. K. Kundu, (2020) *"On the mixed convective carbon nanotube flow over a convectively heated curved surface"* **Heat Transfer *49***(4): 1713–1735. DOI: 10.1002/htj.21687.

[10] B. Mahanthesh, B. J. Gireesha, N. S. Shashikumar, and S. A. Shehzad, (2017) *"Marangoni convective MHD flow of SWCNT and MWCNT nanoliquids due to a disk with solar radiation and irregular heat source"* **Physica E: Low-Dimensional Systems and Nanostructures *94***: 25–30. DOI: 10.1016/j.physe.2017.07.011.

[11] N. S. Shashikumar, B. J. Gireesha, B. Mahanthesh, and B. C. Prasannakumara, (2018) *"Brinkman-Forchheimer flow of SWCNT and MWCNT magneto-nanoliquids in a microchannel with multiple slips and Joule heating aspects"* **Multidiscipline Modeling in Materials and Structures *14***(4): 769–786. DOI: 10.1108/MMMS-01-2018-0005.

[12] S. A. Shehzad, B. Mahanthesh, B. J. Gireesha, N. S. Shashikumar, and M. Madhu, (2019) *"Brinkman-Forchheimer slip flow subject to exponential space and thermal-dependent heat source in a microchannel utilizing SWCNT and MWCNT nanoliquids"* **Heat Transfer - Asian Research *48***(5): 1688–1708. DOI: 10.1002/htj.21452.

[13] A. A. Al-Rashed, K. Kalidasan, L. Kolsi, A. Aydi, E. H. Malekshah, A. K. Hussein, and P. Rajesh Kanna, (2018) *"Three-dimensional investigation of the effects of external magnetic field inclination on laminar natural convection heat transfer in CNT–water nanofluid filled cavity"* **Journal of Molecular Liquids *252***: 454–468. DOI: 10.1016/j.molliq.2018.01.006.

[14] Z. H. Khan, W. A. Khan, R. U. Haq, M. Usman, and M. Hamid, (2020) *"Effects of volume fraction on water-based carbon nanotubes flow in a right-angle trapezoidal cavity: FEM based analysis"* **International Communications in Heat and Mass Transfer *116***: DOI: 10.1016/j.icheatmasstransfer.2020.104640.

[15] A. Ebaid and M. A. Al Sharif, (2015) *"Application of laplace transform for the exact effect of a magnetic field on heat transfer of carbon nanotubes-suspended nanofluids"* **Zeitschrift fur Naturforschung - Section A Journal of Physical Sciences *70***(6): 471–475. DOI: 10.1515/zna-2015-0125.

[16] M. Saqib, I. Khan, and S. Shafie, (2018) *"Natural convection channel flow of CMC-based CNTs nanofluid"* **European Physical Journal Plus *133***(12): DOI: 10.1140/epjp/i2018-12340-3.

[17] N. Acharya, (2021) *"Spectral Simulation to Investigate the Effects of Active Passive Controls of Nanoparticles on the Radiative Nanofluidic Transport Over a Spinning Disk"* **Journal of Thermal Science and Engineering Applications *13***(3): DOI: 10.1115/1.4048677.

[18] N. Acharya, (2020) *"Framing the Impacts of Highly Oscillating Magnetic Field on the Ferrofluid Flow Over a Spinning Disk Considering Nanoparticle Diameter and Solid–Liquid Interfacial Layer"* **Journal of Heat Transfer *142***(10): DOI: 10.1115/1.4047503.

[19] P. R. J. Gowda, N. R. Kumar, A. Aldalbahi, A. Issakhov, B. C. Prasannakumara, M. Rahimi-Gorji, and M. Rahaman, (2021) *"Thermophoretic particle deposition in time-dependent flow of hybrid nanofluid over rotating and vertically upward/downward moving disk"* **Surfaces and Interfaces *22***: 100864.

[20] P. G. R. Jayadevamurthy, N. kumar Rangaswamy, B. C. Prasannakumara, and K. S. Nisar, (2020) *"Emphasis on unsteady dynamics of bioconvective hybrid nanofluid flow over an upward–downward moving rotating disk"* **Numerical Methods for Partial Differential Equations**: DOI: 10.1002/num.22680.

[21] N. Acharya, S. Maity, and P. K. Kundu, (2019) *"Framing the hydrothermal features of magnetized TiO2–CoFe2O4 water-based steady hybrid nanofluid flow over a radiative revolving disk"* **Multidiscipline Modeling in Materials and Structures *16***(4): 765–790. DOI: 10.1108/MMMS-08-2019-0151.

[22] N. Acharya, K. Das, and P. K. Kundu, (2018) *"Rotating flow of carbon nanotube over a stretching surface in the presence of magnetic field: A comparative study"* **Applied Nanoscience (Switzerland) *8***(3): 369–378. DOI: 10.1007/s13204-018-0794-9.

[23] F. Rehman, M. I. Khan, M. Sadiq, and A. Malook, (2017) *"MHD flow of carbon in micropolar nanofluid with convective heat transfer in the rotating frame"* **Journal of Molecular Liquids *231***: 353–363. DOI: 10.1016/j.molliq.2017.02.022.

[24] B. Mahanthesh, B. J. Gireesha, I. L. Animasaun, T. Muhammad, and N. S. Shashikumar, (2019) *"MHD flow of SWCNT and MWCNT nanoliquids past a rotating stretchable disk with thermal and exponential space dependent heat source"* **Physica Scripta *94***(8): DOI: 10.1088/1402-4896/ab18ba.

[25] M. J. Kotresh, G. K. Ramesh, V. K. R. Shashikala, and B. C. Prasannakumara, (2020) *"Assessment of Arrhenius activation energy in stretched flow of nanofluid over a rotating disc"* **Heat Transfer**: DOI: 10.1002/htj.22006.

[26] A. Q. Mohamad, I. Khan, Z. Ismail, and S. Shafie, (2016) *"Exact solutions for unsteady free convection flow over an oscillating plate due to non-coaxial rotation"* **SpringerPlus *5***(1): DOI: 10.1186/s40064-016-3748-2.

[27] H. V. Ersoy. *Effect of magnetic field on the time-dependent flow due to a disk with non-torsional oscillation and a Newtonian fluid at infinity rotating about distinct axes*. 2019. DOI: 10.1007/s12046-019-1132-y.

[28] S. Das, B. Tarafdar, and R. N. Jana, (2018) *"Hall effects on magnetohydrodynamics flow of nanofluids due to non-coaxial rotation of a porous disk and a fluid at infinity"* **Journal of Nanofluids *7***(6): 1172–1186. DOI: 10.1166/jon.2018.1527.

[29] T. S. Ashlin and B. Mahanthesh, (2019) *"Exact solution of non-coaxial rotating and non-linear convective flow of cu–al2 o3 –h2 o hybrid nanofluids over an infinite vertical plate subjected to heat source and radiative heat"* **Journal of Nanofluids *8***(4): 781–794. DOI: 10.1166/jon.2019.1633.

[30] Q. Z. Xue, (2005) *"Model for thermal conductivity of carbon nanotube-based composites"* **Physica B: Condensed Matter *368***(1-4): 302–307. DOI: 10.1016/j.physb.2005.07.024.

[31] H. Villinger, (1985) *"Solving cylindrical geothermal problems using the Gaver-Stehfest inverse Laplace transform."* **Geophysics *50***(10): 1581–1587. DOI: 10.1190/1.1441848.

[32] H. Stehfest, (1970) *"Algorithm 368: Numerical inversion of Laplace transforms [D5]"* **Communications of the ACM *13***(1): 47–49. DOI: 10.1145/361953.361969.